ECS Transactions, 58 (2) 265-274 (2013)
10.1149/05802.0265ecst ©The Electrochemical Society

Dependence of Defect Chemistry and Surface Composition on the Crystal Orientation of $(La_{0.5}Sr_{0.5})_2CoO_4$ Dense Thin Films

Yan Chen,[†] Zhuhua Cai[†] and Bilge Yildiz[*]

Laboratory for Electrochemical Interfaces
Department of Nuclear Science and Engineering, Massachusetts Institute of Technology,
77 Massachusetts Avenue, Cambridge, MA 02139, USA
[†] These authors contributed equally, [*] byildiz@mit.edu

The dependence of oxygen non-stoichiometry on crystal orientation for $(La_{0.5}Sr_{0.5})_2CoO_4$ was investigated by measuring the structure and Co valence state in thin films with (001) and (100) out of plane orientations using X-ray diffraction and X-ray photoelectron spectroscopy. Because of the constraint along the c-axis imposed by the substrate, the c-axis lattice parameter and unit cell volume of the (100) film showed only negligible change when the annealing environment changed from air to ultra-high vacuum (UHV) at elevated temperatures. On the other hand, for the (001) films, the c-parameter and unit cell volume were larger for films annealed in UHV. While the reduced state, Co^{2+}, was detected in the (001) film at 700 ^oC in UHV, Co^{3+} valence state was dominant in the (100) film. These results indicated that the (001) oriented $(La_{0.5}Sr_{0.5})_2CoO_4$ is more reducible compared with (100) oriented ones. The surface composition was found to also depend on orientation, with more A-site enrichment on (100) films.

Introduction

Solid Oxide Fuel Cells (SOFC) are considered to play an essential role in building up a sustainable energy strategy because of their fuel flexibility and very high conversion efficiency (1). To decrease the price and enhance the stability, the working temperature of SOFC needs to decrease from higher than 800 ^oC to intermediate range (500 to 700 ^oC). However, at reduced temperature, the sluggish oxygen reduction reaction (ORR) becomes the main barrier for the SOFC to achieve high efficiency. Therefore, novel cathode materials that can have high ORR reactivity at low temperature are needed. Ruddlesden-Popper (RP) phase oxides are a series of materials with chemical equation of $A_{n+1}B_nO_{3n+1}$, which contains n perovskite layers interweaved with a rock salt (AO) layer in the structure. RP phase oxides as SOFC cathodes exhibit comparable, or even better, ORR reactivity as the state of art perovskite oxide cathodes, especially at the intermediate temperature range (2,3).

The most unique feature of RP phase is the anisotropic diffusion and ORR kinetics which is due to the layered structure. Both experimental and theoretical works showed that the oxygen diffusion along the ab plane (001) in RP phase structure was orders of magnitude faster than that alone the c axis (<001> direction) (2,4)(5-8)(9,10)(11,12). By ab initio calculations, Han and Yildiz (12) reported that, besides the anisotropic diffusion,

the oxygen adsorption and incorporation were also anisotropic, i.e. oxygen adsorption and incorporation on the perfectly terminated (100) surface is more favorable than on the perfectly terminated (001) surface. The interstitial incorporation and interstitiacy diffusion process along the rock-salt layers were believed to be the reason for the fast oxygen incorporation and diffusion path. Considering the very anisotropic ORR kinetics, large variation in ORR activity is expected to exist for the surfaces with different crystal orientation. Therefore, one straight forward approach to synthesize high performance SOFC cathodes using RP phase materials is to utilize the fast oxygen incorporation and diffusion path through the control of surface orientation. While it is difficult to obtain bulk materials which have free surfaces with a specific orientation, as the development of thin film fabrication technique, it is now possible to obtain thin film with controllable crystal structure.(13,14) However, compared with bulk materials, thin films may present very different defect chemistries (15), electronic structures (16) and surface compositions (17,18), all of which directly determine the ORR kinetics. To design a high performance cathode material using a RP thin film with a controllable orientation, we need to understand how those properties vary as a function of crystal orientation in thin film structures, and how such variation impact the ORR reactivity.

The objective of this work is to understand the impact of crystal orientation on the oxygen non-stoichiometry and chemical composition, and how these properties potentially lead to different ORR reactivity on RP phase oxide dense thin films. The model system we choose to study is $(La_{0.5}Sr_{0.5})_2CoO_4$ (LSC_{214}). Strong anisotropic oxygen incorporation and diffusion kinetics were predicted to exist in LSC_{214} by our previous theoretical works.(12) The ORR reactivity on the (100) surface was estimated to be three orders of magnitude higher than the one on (001) surface at 500 ^oC if only a free surface is considered. In this work, ex-situ high resolution X-ray diffraction was used to study the structure change of (100) and (001) films after annealing at high temperature in air and in UHV. We found that the c axis of (100) films was constrained by the substrate. Both c lattice parameter and unit cell volume showed negligible change when the heating environment changes from air to UHV. On the contrary, for the (001) film, in which the c axis is perpendicular to the surface, the c lattice parameter and unit cell volume was much larger for UHV annealed films than the ones annealed in O_2. High temperature X-ray photoelectron Spectroscopy (XPS) was used to study the Co valence state, a parameter determined by the oxygen non-stoichiometry, as a function of temperature in UHV. The Co was found to be more reduced in (001) oriented film at 700 ^oC compared the one with (100) orientation, which indicate less oxygen non-toichiometry on the surface of (001) film compared with the one with (100) orientation at the same temperature in UHV. Combined the XRD results and Co valence state information, the (001) films were found to lose more oxygen than that in (100) film upon heating in UHV. These results suggest that the external strain imposed by substrates on the c axis plays an important role in determining the oxygen nonstoichiometry, which is in consistent with our recent finding on Nd_2NiO_4.(19) The difference in surface compositions between (001) and (100) films were also studied by XPS and correlated to lattice parameters.

Experiment

Two different single-crystal substrates $SrTiO_3$ (001) (STO, a = c = 3.905 Å) and $SrLaAlO_3$ (100) (SLAO, a = 3.756 Å, c=12.636 Å) (MTI Corporation, Richmond, CA)

were used to produce single crystalline LSC_{214} films with (001) and (100) crystal orientations, respectively. The thickness of both films is about 70nm. The (001) film is with the *ab* plane parallel to the surface and c axis perpendicular to the surface, while LSC_{214} (100) is with c axis parallel surface, as shown in Fig. 1. The pulsed laser deposition (PLD) deposition was carried out at 700 °C with O_2 pressure (P_{O2}) of 10 mTorr. The laser beam energy was set at 400 mJ per pulse and 10 Hz pulse frequency. After deposition, the sample was cooled at 5 °C/min to room temperature under a P_{O2} of 2 Torr.

High resolution X-ray diffraction (HR-XRD) measurements were performed employing a high resolution four circle Bruker D8 Discover diffracometer, which is equipped with a Göbel mirror, four-bounce Ge(022) channel-cut monochromator, Eulerian cradle, and a scintillation counter, using Cu $K\alpha_1$ radiation. XRD results of the as-deposited LSC films grown on STO and SLAO substrates, hereafter denoted as (001) and (100) films, exhibited only (00*l*) and (*h00)* diffraction respectively.

The surface chemical composition and Co valence state at elevated temperature was probed using XPS with the Omicron EA 125 hemispherical analyzer and Omicron DAR 400 Mg/Al dual anode non-monochromated X-ray source. Mg K x-ray (1253.6 eV) operated at 300 W was used in the XPS measurements reported here. Casa XPS 2.3.15 software was used to assess the spectra and calculate the relative intensity of each constituent by employing the Shirley background. The Sr 3*d*, La *4d*, La 3*d* and Co 2*p* photoelectron were analyzed.

Results and Discussion

Defect Chemistry versus Structure

In the following part, we study the difference in defect chemistry between (100) and (001) films by checking their structure change with oxygen non-stoichiometry. The oxygen non-stoichiometry of a thin film changes with the oxygen gas pressure to keep the chemical potential of oxygen in the film the same as the oxygen gas chemical potential near the surface. While it is difficult to control oxygen non-stoichiometry precisely, especially in the case of thin film, it is much easier to control the oxygen gas chemical potential near the surface, which is the driving force for the change of film oxygen content. Therefore, to introduce variation in oxygen nonstoichiometric in the film, we annealed both (001) and (100) films at the same time in air at 800 ^oC, and in ultra-high vacuum (UHV, ~10^{-9} mbar) at 700 ^oC for 1 hour. Because the much lower oxygen gas chemical potential in UHV condition compared with that in air, both (001) and (100) films have less oxygen content in UHV annealing films compared with air annealed ones. After cooling the samples down to room temperature, the different oxygen non-stoichiometry in UHV annealed and air annealed samples can partly sustain in the films. Such changes in oxygen non-stoichiometry directly impact film structure. We use HR-XRD to study the structure difference between UHV annealed and air annealed films to indirectly extract information about the oxygen non-stoichiometry change when the films went from air annealing condition to UHV annealing condition.

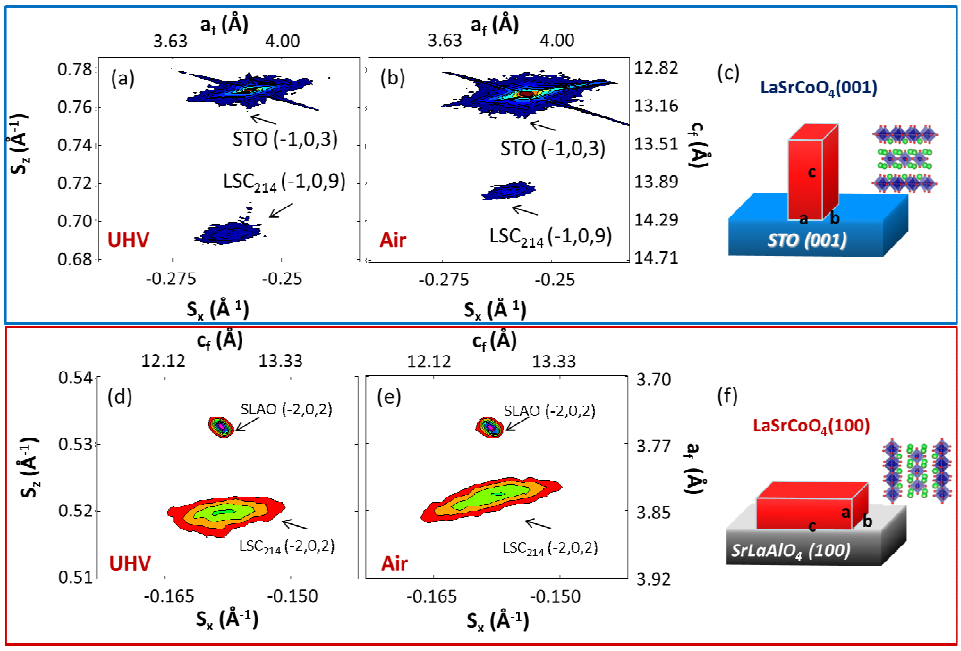

Figure 1. **(a-b)** Reciprocal space maps of (-1,0,3) on the LSC_{214} (001) film grown on $SrTiO_3$(STO) substrate after annealing, with STO (-1,0,9) reference reflection (a) in ultra-high vacuum (UHV) at 700 ^oC (b) in air at 800 ^oC; **(c)** schematic figure shows the crystal structure orientation of LSC_{214} (001) films on STO; **(d-e)** Reciprocal space maps of (-2,0,2) LSC_{214} (100) film grown on $SrLaAlO_4$(SLAO) substrate after annealing, with SLAO (-2,0,2) reference reflection peak (d) in ultra-high vacuum (UHV) at 700 ^oC (e) in air at 800 ^oC; **(f)** schematic figure shows the crystal structure orientation of LSC_{214} (100) films on SLAO.

Fig. 1 is the reciprocal map results of LSC_{214} (001) and (100) films after UHV and air annealing, together with their crystal structure. The in plane and out of plane lattice parameter of LSC_{214} thin film annealed in UHV and in air were determined through checking the position of film peak in the reciprocal map with substrate peak as a reference. For (001) film on STO, the LSC_{214} (-1,0,3) reflection peak is used to determine the in plane parameters a and b, and out of plane parameters c, while STO (-1,0,9) reflection peak is used as a reference peak to avoid systematic error. What shown in Fig. 1 (a) and (b) are the (-1,0,3) reflection peak of (001) film and (-1,0,9) peak of STO substrate. The (-1,0,3) reflection peak for the UHV annealed (001) film is much further away from the STO reference peak in z direction compared with that of air annealed (001) film. This indicated much larger c parameters for UHV annealed sample. Such change can be seen more clearly in Fig.2 (a), where both in plane and out of plane the lattice parameters are plotted as a function of annealing environment. For UHV annealed LSC_{214} (001) sample, c parameters is 13.00 **Å**, which is much larger than 12.53 **Å** for air annealed one. From Fig.1 (a) and (b), we can see that the (-1,0,9) reflection peak of both LSC_{214} (001) film annealed in UHV and in air are not vertically aligned to the substrate (-1,0,3) peak, which indicate that they are not full strained by STO substrate. As shown in Fig. 2 (a), the in-plane a and b parameters are smaller than the lattice parameter of STO 3.905 Å for both air annealed and UHV annealed (001) films. There is no apparent difference between for air and UHV annealed sample in a and b value, 3.84 Å for the UHV annealed films and 3.85 **Å** for the air annealed ones. The XRD results indicate that when (001) films lose oxygen by going from annealing at high temperature in air to annealing in UHV, the out of plane c parameter shows significant expansion, while the in

plane a and b parameter show negligible change. As shown in Fig.2 (c), the unit cell volume of UHV annealed (001) films is larger than that of air annealed ones, which follow the trend for c parameters.

For the LSC_{214} (100) film, (-2,0,2) reflection peak is used to determine the c parameter that is parallel to the surface and the out of plane lattice parameters a, shown in Fig. 1 (d-e). The in plane lattice parameter b and out of plane a of (100) films are determined using LSC_{214} (2,4,0) reflection peak, which is not shown here, with SLAO (2,4,0) reflection peak as reference. The in plane c parameters of LSC_{214} (001) / SLAO after annealing in UHV and air are found to have the similar value, which is close to the c parameter for SLAO substrate, as shown in the dash-dot line in Fig. 2 (b). From Fig. 2 (b) we can also see that another in plane parameter b for air and UHV annealing cases are similar. The out of plane lattice parameter a for the UHV annealed LSC (100) sample is slightly larger than that of the air annealed sample. This indicates that, similar to the case of the (001) films, the in plane lattice parameters of LSC (100) on SLAO are fixed by the substrate and show negligible change over the variation of oxygen non-stoichiometry. Any stoichiometry difference between LSC (100) annealed in UHV and in air are accommodated by the slightly change in the out of plane parameters a.

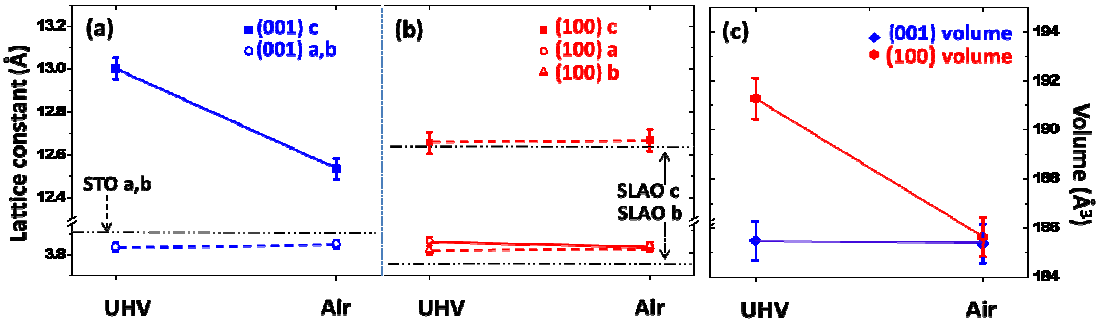

Figure 2. Variation of lattice parameter for LSC_{214} (001)/STO and LSC_{214} (100)/SLAO films upon UHV annealing and Air annealing. (a) for LSC_{214} (001)/STO ; (b) for LSC_{214} (001)/STO. The data points connected by solid line are corresponding to out of plane parameter: c for LSC_{214} (001) and a for LSC_{214} (100), while the data point connected with dash line are corresponding to in plane parameter: a and b for LSC (001); c and b for (100). For comparison, the in plane lattice parameter of STO and SLAO substrate are marked as black dash-dot horizontal line in the figures; **(c)** Comparison of unit cell volume for LSC_{214} (001) and (100) film upon annealing in UHV and in air.

It has been well known that the defect chemistry of oxide cathodes is one of the most important features to determine the ORR kinetics.(20) In RP phase oxides, the oxygen defects can exist in the both forms of oxygen vacancy $V_O^{\square}$ and oxygen interstitials $O_i^{"}$. The amount of these oxygen defect ($V_O^{\square}$ and $O_i^{"}$) depends on the oxygen non-stoichiometry in the film, a parameter that determined by the oxygen partial pressure near the surface or external bias. It has been widely observed in oxides that the changes in oxygen non-stoichiometry are accompanied by the change in the structure.(21-23) In RP phases, such changes in structure is anisotropic in c direction (<001> direction) and over ab plane. Intensive works has been done on bulk RP phase oxide to determine the correlation between the oxygen non-stoichiometry and lattice parameter, especially c parameter. (24-

26) (27) (28,29) The change in c parameter not only depends on absolute value of oxygen content but also on the type of oxygen defects that created. While the c parameter is reported to decrease (24-26)(27) (28,29) when the RP phase oxides lose oxygen in the form of oxygen interstitial, it increases when the loss of oxygen is in the form of creating oxygen vacancies.(25,27) All these results indicate that the oxygen insertion/extraction process induces large change in the structure, especially along c axis. In thin film geometry, on the other hand, the existences of substrate constrain the in-plane structure change over change in oxygen non-stoichiometry. We observed large increase of c parameter and unit cell volume in (001) films when the film lose oxygen by going from air annealing case to UHV annealing case. Such increases were expected to be induced by the formation of oxygen vacancies after UHV annealing. On the other hand, (100) films showed negligible changes in c parameter and in unit cell volume, which we believe is because of the constraint of substrate over c parameter. Our results showed that the presence of substrate constrain the in plane structure change over change in non-stoichiometry. Such constraint can potentially influence oxygen insertion and extraction process, which in turn impact the oxygen reduction kinetics.

Defect Chemistry versus Co Valence State

Co oxidation states are the other properties we used to monitor the relative presence of surface oxygen vacancies on the LSC_{214} films. Fig. 3 shows the Co 2p XPS spectra of (001) and (100) films at different temperature in UHV conditions. At room temperature, both film surfaces had mainly Co^{3+}. This is deduced from presence of a weak satellite feature at around 790 eV that is characteristic of a mixed Co^{2+} and Co^{3+} state as in Co_3O_4,(30) and the smaller magnitude of this peak at 790 eV suggests more dominance of the Co^{3+} state. As shown in Figure 3(a), for the LSC_{214}(001), the Co^{2+} satellite peak (31,32) at around 786 eV was evident already at 600 °C, suggesting the enhanced formation of Co^{2+} due to the oxygen vacancies. In comparison, the Co 2*p* spectra at 600 °C and 800 °C for the LSC_{214} (100) showed a mainly Co^{3+} line shape (31,33) without an evident Co^{2+} satellite feature for the same duration of annealing (Figure 3(b)). The absence of Co^{2+} satellite peaks in the spectra from (100) films may result from only a small amount of Co^{2+} formation (that our measurements were not sensitive to) or only the reduction of Co^{4+} to Co^{3+} that could inherently not be distinguished from the Co 2*p* emission by the sensitivity of the XPS technique. The difference in Co valence state suggests a difference in the oxygen non-stoichiometry of these differently oriented films, with an enhanced formation of oxygen vacancies near the surface of the (100) films. Our XPS results is in consistent with the XRD results shown in previous session, which both shows that the oxygen non-stoichiometry in (001) film are less than that in (100) film under UHV annealing condition.

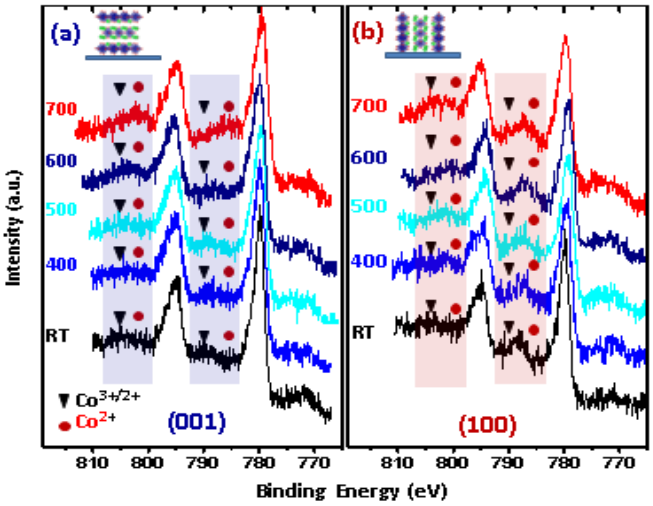

Figure 3. Co 2*p* region of the photoelectron spectra on (a) LSC_{214} (001) and (b) LSC_{214} (100) at room temperature up to 700ºC. Satellite peaks (Sat.) represent the enhanced presence of Co^{2+} oxidation state in addition to the Co^{3+} state. The Co 2*p* spectra shows enhanced formation of Co^{2+} on the LSC_{214}(001) films compared to the LSC_{214}(100) at elevated temperatures.

Surface Composition

The Sr content on the A-site (quantified as Sr/(Sr+La)), and the relative presence of A-site versus B-site cations (quantified as (Sr+La)/Co)) on the LSC_{214} surface were assessed by analyzing the Sr 3*d*, La 3*d*, La 4*d*, and Co 2*p* emissions in the XPS measurements. At room temperature, the Sr/(Sr+La) ratios of 0.59 ± 0.02 and 0.58 ± 0.02 found for (001) film and (100) film respectively, show an enhanced presence of Sr cations on the A-site on both of the LSC_{214} film surfaces. The (Sr+La)/Co ratio on the surface of (001) and (100) film as a function of UHV and air annealing temperature are shown in Fig. 4, which indicate strongly AO-terminated surfaces (A = La, Sr). LSC_{214} (001) showed much lower (Sr+La)/Co ratio than LSC_{214} (100), suggesting lower A-site segregation.

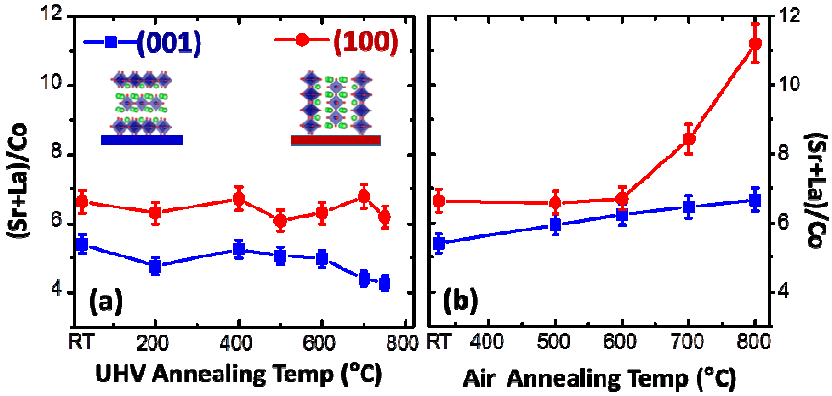

Figure 4.(Sr+La)/Co ratios on LSC_{214}(001) and (100) changing with temperature in (a) ultra-high vacuum condition (b) and in air, deduced from the x-ray photoelectron spectroscopy measurements.

When these two films were annealed in vacuum (i.e. 2×10^{-9}Torr), there was no noticeable change in cation concentration ratios, from room temperature up to 750 ºC. Comparing to vacuum annealing, annealing in air showed much higher A site segregation. Comparing to LSC_{214} (001), LSC_{214} (100) showed significant A site cation segregation at annealing temperature higher than 600°C, suggesting much higher tendency of cation segregation of (100) film than that of the (001) films.

Surface composition of a thin film oxide is another important character of determining the oxygen reduction kinetics. For perovskite oxide, surface segregation is widely studied (18,34-38) and has been proved to be directly related to the surface ORR activities, as demonstrated in materials like $Sr(Ti,Fe)O_3$ (STF), LSC_{113}, $(La,Sr)MnO_3$ (LSM)(16,18,38-41) and so on. Here we reported much larger cation segregation on (100) films compared with (001) films. Such variation in surface chemistry can be another factor, other than defect chemistry mentioned in the previous session, greatly impact the ORR activities.

Conclusion

Epitaxial LSC_{214} film with (100) and (001) out of plane orientation were successfully synthesized by PLD on STO (001) and SLAO (100) substrate. Ex-situ HR-XRD is used to study the structure of (100) and (001) films after annealing at high temperature in air and in UHV. The c axis of (100) films was found to be constrained by the substrate. Consequently, both the c parameter and the unit cell volume showed negligible change when the heating environment changes from air to UHV. On the contrary, for (001) film whose c axis is perpendicular to the surface, the c parameter and unit cell volume was much larger for UHV annealed films compared with the ones annealed in air. Such increases of c parameter and unit cell volume are considered to be induced by the formation of oxygen vacancies. These results indicate more loss of oxygen in the (001) films compared to the (100) films when they are annealed in UHV. High temperature XPS results showed the present of Co^{2+} in (001) film at 700 ^{o}C in UHV, while no detectable Co^{2+} formed in (100) film at the same condition. Both XRD and XPS results indicates different defect chemistry between (100) and (001) films. Besides defect chemistry, the surface composition were also found to be different on (001) and (100) surface. More A site segregation were observed in (100) films. Our results about the dependence of the defect chemistry and surface composition on the surface orientation of LSC_{214} thin films are important to understand the dependence of ORR activity on the surface orientation of RP phase thin films. Such understanding is helpful for future design of high performance SOFC cathodes materials.

Acknowledgments

We gratefully acknowledge financial support of this research from Low Carbon Energy University Alliance of Tsinghua-MIT-Cambridge Universities, supported by Chinese government; and we also thank Prof. C. Ross and Prof. H. L. Tuller at MIT for the use of the PLD system.

References

1. E. D. Wachsman, C. A. Marlowe and K. T. Lee. *Energy & Environmental Science* **5**, 5498 (2012).
2. E. Boehm, J. M. Bassat, P. Dordor, F. Mauvy, J. C. Grenier and P. Stevens. *Solid State Ionics* **176**, 2717 (2005).
3. L. W. Tai, M. M. Nasrallah, H. U. Anderson, D. M. Sparlin and S. R. Sehlin. *Solid State Ionics* **76**, 259 (1995).
4. C. N. Munnings, S. J. Skinner, G. Amow, P. S. Whitfield and I. J. Davidson. *Solid State Ionics* **176**, 1895 (2005).
5. A. Kushima, D. Parfitt, A. Chroneos, B. Yildiz, J. A. Kilner and R. W. Grimes. *Physical Chemistry Chemical Physics* **13**, 2242 (2011).
6. M. B. Albert Tarancón , José Santiso , Stephen J. Skinner and John A. Kilner *Journal of Materials Chemistry* **20**, 3799 (2010).
7. B. Y. Jeong Woo Han. *Energy & Environmental Science* (2012).
8. M. Burriel, G. Garcia, J. Santiso, J. A. Kilner, R. J. Chater and S. J. Skinner. *Journal of Materials Chemistry* **18**, 416 (2008).
9. J. M. Bassat, P. Odier, A. Villesuzanne, C. Marin and M. Pouchard. *Solid State Ionics* **167**, 341 (2004).
10. M. Burriel, G. Garcia, J. Santiso, J. A. Kilner, J. C. C. Richard and S. J. Skinner. *Journal of Materials Chemistry* **18**, 416 (2008).
11. J. M. Bassat, P. Odier, A. Villesuzanne, C. Marin and M. Pouchard. *Solid State Ionics* **167**, 341 (2004).
12. J. W. Han and B. Yildiz. *Energy & Environmental Science* **5**, 8598 (2012).
13. J. Santiso and M. Burriel. *Journal of Solid State Electrochemistry* **15**, 985.
14. D. Beckel, A. Bieberle-Hutter, A. Harvey, A. Infortuna, U. P. Muecke, M. Prestat, J. L. M. Rupp and L. J. Gauckler. *Journal of Power Sources* **173**, 325 (2007).
15. G. J. la O, R. F. Savinell and Y. Shao-Horn. *Journal of the Electrochemical Society* **156**, B771 (2009).
16. Y. Chen, W. C. Jung, Z. Cai, J. J. Kim, H. Tuller and B. Yildiz. *Energy & Environmental Science* **5**, 7979 (2012).
17. Z. H. Cai, Y. Kuru, J. W. Han, Y. Chen and B. Yildiz. *Journal of the American Chemical Society* **133**, 17696 (2011).
18. W. Lee, J. W. Han, Y. Chen, Z. Cai and B. Yildiz. *Journal of the American Chemical Society* **135**, 7909 (2013).
19. N. Tsvetkov, Q. Lu, Y. Chen and B. Yildiz. *submitted* (2013).
20. S. B. Adler. *Chemical Reviews* **104**, 4791 (2004).
21. D. Marrocchelli, S. R. Bishop, H. L. Tuller and B. Yildiz. *Advanced Functional Materials* **22**, 1958 (2012).

22. D. Marrocchelli, S. R. Bishop, H. L. Tuller, G. W. Watson and B. Yildiz. *Physical Chemistry Chemical Physics* **14**, 12070 (2012).

23. Y. Kuru, S. R. Bishop, J. J. Kim, B. Yildiz and H. L. Tuller. *Solid State Ionics* **193**, 1.

24. T. Nakamura, K. Yashiro, K. Sato and J. Mizusaki. *Solid State Ionics* **180**, 1406 (2009).

25. T. Nakamura, K. Yashiro, K. Sato and J. Mizusaki. *Solid State Ionics* **181**, 292 (2010).

26. V. V. Kharton, A. V. Kovalevsky, M. Avdeev, E. V. Tsipis, M. V. Patrakeev, A. A. Yaremchenko, E. N. Naumovich and J. R. Frade. *Chemistry of Materials* **19**, 2027 (2007).

27. T. Nakamura, K. Yashiro, K. Sato and J. Mizusaki. *Solid State Ionics* **181**, 402 (2010).

28. V. V. Kharton, M. V. Patrakeev, E. V. Tsipis, M. Avdeev, E. N. Naumovich, P. V. Anikina and J. C. Waerenborgh. *Solid State Ionics* **181**, 1052 (2010).

29. L. V. Mogni, F. D. Prado, G. J. Cuello and A. Caneiro. *Chemistry of Materials* **21**, 2614 (2009).

30. C. A. F. Vaz, D. Prabhakaran, E. I. Altman and V. E. Henrich. *Physical Review B* **80**, 155457 (2009).

31. S. C. Petitto, E. M. Marsh, G. A. Carson and M. A. Langell. *Journal of Molecular Catalysis a-Chemical* **281**, 49 (2008).

32. J. G. Kim, D. L. Pugmire, D. Battaglia and M. A. Langell. *Applied Surface Science* **165**, 70 (2000).

33. C. A. F. Vaz, D. Prabhakaran, E. I. Altman and V. E. Henrich. *Phys. Rev. B* **80**, 155457 (2009).

34. K. Szot, M. Pawelczyk, J. Herion, C. Freiburg, J. Albers, R. Waser, J. Hulliger, J. Kwapulinski and J. Dec. *Applied Physics a-Materials Science & Processing* **62**, 335 (1996).

35. T. T. Fister, D. D. Fong, J. A. Eastman, P. M. Baldo, M. J. Highland, P. H. Fuoss, K. R. Balasubramaniam, J. C. Meador and P. A. Salvador. *Applied Physics Letters* **93**, 151904 (2008).

36. C. N. Borca, B. Xu, T. Komesu, H. K. Jeong, M. T. Liu, S. H. Liou and P. A. Dowben. *Surface Science* **512**, L346 (2002).

37. H. Dulli, E. W. Plummer, P. A. Dowben, J. Choi and S. H. Liou. *Applied Physics Letters* **77**, 570 (2000).

38. W. Jung and H. L. Tuller. *Energy & Environmental Science* **5**, 5370 (2011).

39. Z. Cai, M. Kubicek, J. Fleig and B. Yildiz. *Chemistry of Materials* (2012).

40. M. Kubicek, A. Limbeck, T. Fromling, H. Hutter and J. Fleig. *Journal of the Electrochemical Society* **158**, B727 (2011).

41. S. P. Jiang and J. G. Love. *Solid State Ionics* **138**, 183 (2001).